Supporting Online Materials

Methods

Lipidic cubic phase crystallization

Crystals of engineered human β_2AR (β_2AR-T4L) grown from bicelles could not be optimized beyond 3.5 Å resolution after extensive screening (Supplementary Figure S1). For lipidic cubic phase (LCP) crystallization trials, robotic trials were performed using an *in meso* crystallization robot (*S1*). 96-well glass sandwich plates (*S1, S2*) were filled with 25 or 50 nL protein-laden LCP drops overlaid by 0.8 μL of precipitant solution in each well and sealed with a glass coverslip. All operations starting from mixing lipid and protein were performed at room temperature (~21-23 °C). Crystals were obtained in 30-35% (v/v) PEG 400, 0.1-0.2 M sodium sulfate, 0.1 M Bis-tris propane pH 6.5-7.0 and 5-7% (v/v) 1,4-butanediol using 8-10% (w/w) cholesterol in monoolein as the host lipid (Supplementary Figure S2A). PEG 400 and sulfate ion were essential for crystallization, while addition of cholesterol and 1,4-butanediol dramatically improved crystals size and shape enabling high-resolution diffraction. Additions of phospholipids (dioleoylphosphatidylcholine, dioleoylphosphatidylethanolamine, asolectin) alone and in combinations with cholesterol to the main host LCP lipid monoolein were tried, however, none of them improved crystal quality.

Crystal harvesting

The average size of the harvested crystals was $30 \times 15 \times 5$ μm (largest crystal was $40 \times 20 \times 7$ μm). Crystals were harvested directly from the glass sandwich plates, even though these plates have been specifically designed for screening and optimization (*S1, S2*). Crystals were scooped directly from the LCP using 30 or 50 μm aperture MiTeGen MicroMounts and plunged

into liquid nitrogen. Care was taken to drag as little as possible lipid around the crystal to decrease unwanted background scattering. Attempts to dissolve the lipids, either by increasing concentration of PEG 400 or using a mineral oil, typically resulted in a decrease in diffraction power of the crystals.

Data collection

X-ray data were collected on the 23ID-B beamline (GM/CA CAT) at the Advanced Photon Source, Argonne, IL using a 10 μm minibeam (wavelength 1.0332 Å) and a MarMosaic 300 CCD detector (Supplementary Figure S2B). Several complete datasets were collected from single crystals at resolution between 2.8 and 3.5 Å using 5x attenuated beam, 5 s exposure and 1° oscillation per frame. However, some crystals diffracted to a maximum of 2.2 Å resolution upon 5 s exposure with 1x attenuated beam. Therefore, we collected 10-20° wedges of high-resolution data from more than 40 crystals (some of the crystals were large enough to allow 2-3 translations) and combined 31 of the best datasets together from 27 independent crystals, scaling them against the lower resolution full dataset to obtain complete 2.4 Å data.

One of the challenges during data collection was visualization of colorless microcrystals within an opaque frozen lipid phase and aligning them with the 10 μm minibeam. Without being able to visualize the crystals adequately through the inline optics at the beamline, we resorted to alignment by diffraction. After numerous trial-and-error attempts, an optimized crystal search algorithm was designed to locate the crystals without the minibeam. First, the area of the loop containing lipid was scanned in the vertical direction with a highly attenuated and slitted 100×25 μm beam. When diffraction was found, the crystal location was further confined by two additional exposures to an area of $\sim 50 \times 25$ μm. This area was further coarse-scanned with the collimated and 10x attenuated minibeam using 15 μm steps, following by fine-tuning the position

using 5 and 2 μm steps. After locating the crystal in one orientation the loop was rotated 90° and the procedure was repeated. Typically during alignment the crystal was exposed ~10 times using 10x attenuated beam and 2 s exposures. Work is in progress to develop a fully automated scanning procedure to align invisible microcrystals with the minibeam in place.

Data processing

A 90% complete, 2-fold redundant monoclinic dataset was processed from one crystal diffracting to 2.8 Å resolution. Initial indexing of lattice parameters in spacegroup C2 and crystal orientation were performed using HKL2000 (*S3*). The refined lattice parameters and space group were implemented in the data processing program XDS for spot integration which models error explicitly for radiation decay, absorption, and rotation (*S4*). As we were collecting data using a 10 μm beam from microcrystals, maintaining the crystal orientation at the beam center during data collection was especially problematic. It appeared that XDS modeled the crystal orientation error upon rotation about the phi axis better than other data processing programs that were tried, resulting in better merging statistics. In addition to rotational error, the radiation decay was also an issue that was partially corrected by the XDS processing program, enabling a more reliable scaling of datasets from different crystals and translations of crystals. The 2.8 Å data was used as a scaling reference for incorporation of additional wedges of data collected at a much higher exposure. Each new dataset was indexed in XDS using the original unit cell parameters as constants which were then refined along with the crystal orientation, beam geometry, and mosaicity parameters. The refinement was generally stable, resulting in very similar unit cell constants which enabled subsequent scaling. All of the integrated wedges of data were then tested individually against the scaling reference set and included in the final scaled dataset if the merging statistics remained acceptable upon incorporation of the data. In total, 31 wedges of data

from 27 crystals were combined with the scaling reference dataset, 22 of which diffracted to a resolution of 2.4 Å or better. Each of the higher resolution datasets were exposed to a much larger dose of radiation resulting in a rapid decay in intensity. Typically 10° – 20° wedges were collected from each crystal or translation, 5° – 7° of which had diffraction data to 2.4 Å. The final merging statistics for the dataset are shown in Table S1. Based on the mean $F/\sigma(F)$ of reflections near the three crystallographic axes, we estimate the effective resolution to be 2.4 Å along b* and c* and 2.7 Å along a*. The anisotropy results in the high merging R factors in the last few resolution shells despite the significant $I/\sigma(I)$ values. The anisotropy is either an inherent property of the crystals or the result of a preferential orientation of the crystals within the mounting loop. Thus, the higher resolution shells were filled in anisotropically by incorporation of the additional data at high exposure levels, while the lower resolution shells have a very high redundancy and low anisotropy.

Structure solution and refinement

Initial phases for β_2AR-T4L were obtained by molecular replacement using both T4-lysozyme (PDB ID Code 2LZM) and a polyalanine model of the rhodopsin seven-transmembrane bundle (PDB ID Code 1U19) as search models. It was necessary to trim the lysozyme search model to remove residues 12-71 as that domain had shifted conformations relative to the larger section. This domain was later reintroduced to the model by fitting into observed density. Molecular replacement was carried out using the program Phaser by first placing the truncated lysozyme (RFZ= 3.74; TFZ= 3.65) followed by the rhodopsin model (RFZ= 5.2; TFZ= 7) (*S5*). In order to optimize placement of the receptor each of the seven helices was refined independently by rigid body maximum likelihood refinement as implemented in Refmac (Initial R_{work}/R_{free} = 0.50 / 0.51) (*S6*).

Initial rounds of refinement were carried out using restrained parameters in Refmac. Model rebuilding was performed in Coot utilizing $2F_o$-F_c sigma-A weighted maps, as well as density modified maps calculated using Resolve prime-and-switch phasing which reduces model bias introduced by model based phasing methods (*S7*). During the initial rounds of refinement we observed that the Resolve calculated maps were superior to the sigma-A weighted ones in that more of the main chain density could be traced. Density for the bound ligand was visible early in the refinement but was not modeled immediately to allow an unbiased assessment of the phase quality through the improvement of the signal/noise of the observed ligand density. The structure quality is excellent (Table 1 of the main paper), with strong electron density in particular observed in the ligand binding site (Supplementary Figure S3), cholesterol binding sites (Supplementary Figure S4A), and the proline helix kinks (Supplementary Figure S4B).

References

1.   V. Cherezov, A. Peddi, L. Muthusubramaniam, Y. F. Zheng, M. Caffrey, *Acta Crystallogr D Biol Crystallogr* **60**, 1795 (2004).

2.   V. Cherezov, D. P. Siegel, W. Shaw, S. W. Burgess, M. Caffrey, *J Membr Biol* **195**, 165 (2003).

3.   Z. Otwinowski, W. Minor, in *Methods in Enzymology* C. W. J. Carter, R. M. Sweet, Eds. (Academic Press, New York, 1997), vol. 276, pp. 307-326.

4.   W. Kabsch, *J Appl Crystallogr* **26**, 795 (1993).

5.   A. J. McCoy, *Acta Crystallogr D Biol Crystallogr* **63**, 32 (2007).

6.   G. N. Murshudov, A. A. Vagin, E. J. Dodson, *Acta Crystallogr D* **D53**, 240 (1997).

7.   T. C. Terwilliger, *Acta Crystallogr D* **D56**, 965 (2000).

8.   K. Diederichs, P. A. Karplus, *Nat Struct Mol Biol* **4**, 269 (1997).

Signal/noise ≥ -3

Resolution	# Observed refl	# Unique refl	Redundancy	Completeness	R_{sym}	I/SIGMA	R-meas	Rmrgd-F
10	3352	333	10.1	87.40%	6.60%	23.25	6.90%	2.70%
8	3591	354	10.1	99.40%	7.60%	22.6	8.00%	2.80%
6	10480	1003	10.4	99.60%	9.90%	20.01	10.50%	4.00%
3	126008	11968	10.5	99.80%	13.30%	14.01	14.00%	6.60%
2.8	33158	3130	10.6	100.10%	38.00%	6.42	39.90%	18.70%
2.7	19702	1893	10.4	99.70%	49.50%	4.96	52.10%	24.90%
2.6	23772	2275	10.4	99.90%	60.20%	4.07	63.40%	30.10%
2.5	14108	2558	5.5	99.30%	58.90%	2.69	65.10%	51.80%
2.4	14672	3060	4.8	99.10%	67.80%	2.18	75.70%	62.80%
total	248843	26574	9.4	99.50%	12.70%	9.62	13.40%	11.40%

Signal/noise ≥ 0

Resolution	# Observed refl	# Unique refl	Redundancy	Completeness	R_{sym}	I/SIGMA	R-meas	Rmrgd-F
10	3352	333	10.1	87.40%	6.60%	23.25	6.90%	2.70%
8	3591	354	10.1	99.40%	7.60%	22.6	8.00%	2.80%
6	10480	1003	10.4	99.60%	9.90%	20.01	10.50%	4.00%
3	125628	11923	10.5	99.40%	13.30%	14.06	14.00%	6.50%
2.8	32679	3077	10.6	98.40%	37.60%	6.54	39.50%	17.70%
2.7	19346	1849	10.5	97.40%	48.80%	5.08	51.30%	23.40%
2.6	23201	2210	10.5	97.00%	58.90%	4.2	62.00%	28.00%
2.5	13461	2406	5.6	93.40%	56.40%	2.88	62.30%	45.90%
2.4	13833	2827	4.9	91.50%	64.10%	2.4	71.50%	54.30%
total	245571	25982	9.5	97.30%	12.60%	9.85	13.30%	10.80%

Table S1. Data processing statistics from XDS. A comparison is made between data filtered by a sigma cutoff and the complete set. All of the data was used in structure solution and refinement.

$R_{sym} = \Sigma_{hkl} |I(hkl) - <I(hkl)>| / \Sigma_{hkl}(hkl)$, where $<I(hkl)>$ is the mean of the symmetry equivalent reflections of I(hkl)

R-meas = redundancy independent Rsym; Rmrgd-F= indication of amplitude quality (*S8*).

Table S2: Direct contacts between β_2AR and T4L

van der Waals Contacts	
β_2AR atom	T4 Lysozyme
Leu230$^{5.69}$	Trp158
Lys263$^{6.25}$	Asp159
Cys265$^{6.27}$	Ile9
Leu266$^{6.28}$	Ile9
Leu266$^{6.28}$	Glu5

Hydrogen Bond and Salt Bridge Contacts		
β_2AR atom	T4 Lysozyme	Distance (Å)
Lys227$^{5.66}$(NZ)	Asp159(OD1)	3.4
Gln229$^{5.68}$(O)	Asn2 (N)	3.1
Gln229$^{5.68}$(O)	Asn2 (ND2)	3.2
Glu268$^{6.30}$(OE2)	Arg8 (NH2)	3.2

Covalent bonds	
β_2AR atom	T4 Lysozyme
Leu230$^{5.69}$	Asn2
Lys263$^{6.25}$	Tyr161

Table S3: Direct contacts between β_2AR and carazolol.

Hydrogen Bond and Salt Bridge Contacts

β_2AR atom	Carazolol	Distance (Å)
Asp113$^{3.32}$ (OD2)	N19	2.9
Asp113$^{3.32}$ (OD1)	O17	2.6
Ser203$^{5.42}$ (OG)	N7	3.2
Asn312$^{7.39}$ (ND2)	O17	2.9
Asn312$^{7.39}$ (OD1)	N19	2.9
Tyr316$^{7.43}$ (OH)	N19	3.4

Hydrophobic and Aromatic Interactions
(closest distance for each residue, <4 Å)

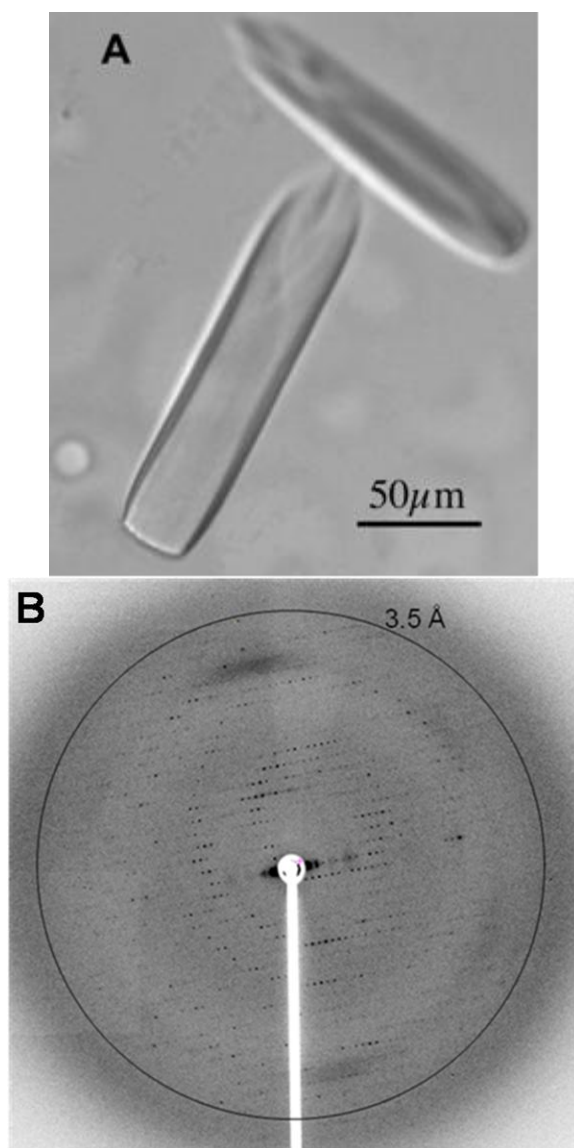| β_2AR atom	Carazolol	Distance (Å)
Trp109$^{3.28}$ (CH2)	C21	3.8
Val114$^{3.33}$ (CG1)	C11	3.9
Val117$^{3.36}$ (CG1)	C12	4.0
Thr118$^{3.37}$ (OG1)	C11	3.9
Phe193$^{5.32}$ (CE2)	C6	3.5
Tyr199$^{5.38}$ (CE2)	C2	3.9
Ser207$^{5.46}$ (CB)	C10	3.6
Trp286$^{6.48}$ (CH2)	O17	3.4
Phe289$^{6.51}$ (CE2)	O14	3.7
Phe290$^{6.52}$ (CZ)	C12	3.5
Asn293$^{6.55}$ (ND2)	C5	3.6
Tyr308$^{7.35}$ (OH)	C6	3.6

Supporting Online Figures

Figure S1. **A.** β₂AR-T4L Crystals grown from bicelle conditions. **B.** Diffraction image from bicelle grown microcrystals of β₂AR-T4L recorded using 10 μm minibeam on 23ID-B beamline at APS. Black circle is drawn at resolution 3.5 Å.
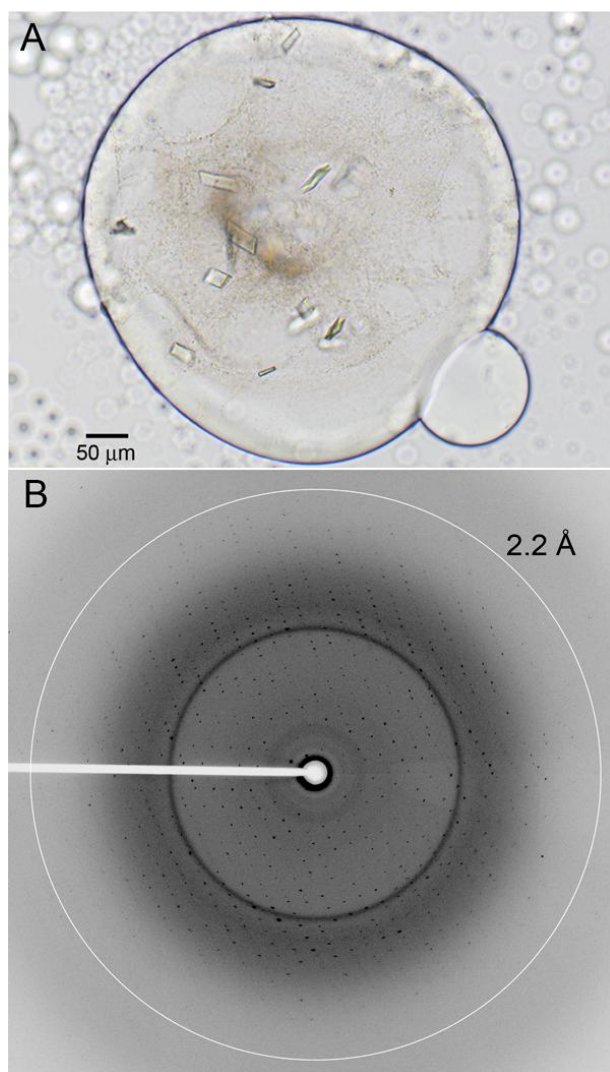
Figure S2. **A.** Microcrystals of β_2AR-T4L grown in lipidic mesophase. **B.** Diffraction image from lipidic cubic phase grown microcrystals of β_2AR-T4L recorded using a 10 µm minibeam on 23ID-B beamline at APS. The white circle is drawn at resolution 2.2 Å.
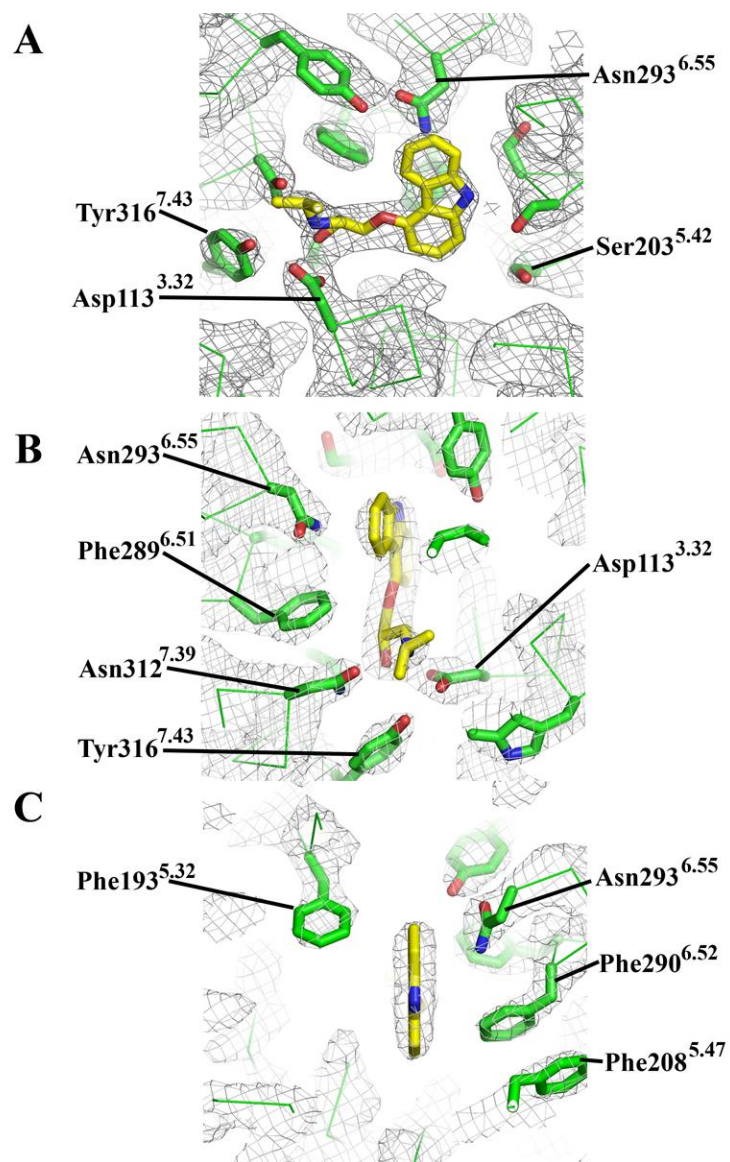
Figure S3. Detailed representation of the carazolol binding site in β_2AR-T4L. **A, B, and C.** Electron density representations of the ligand binding site at three different orientations. Residues are labeled by their Ballesteros-Weinstein numbers as superscripts. Electon density is contoured at 1σ from a 2F_o-F_c difference map. Both **B** and **C** are generated by rotating the field of view 90° about the y-axis clockwise and counterclockwise respectively.
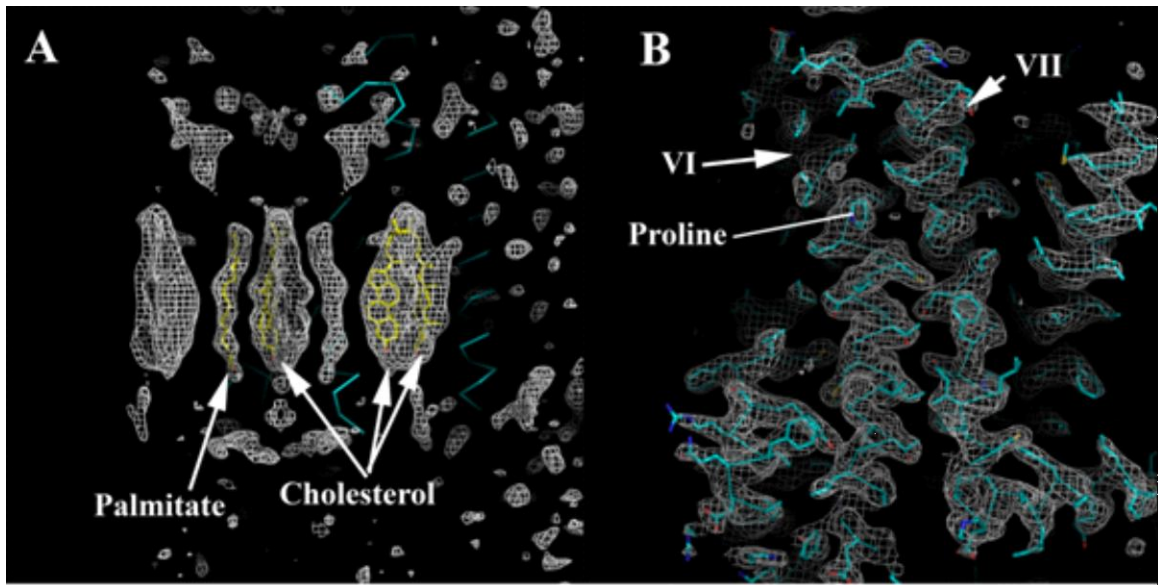
Figure S4. Electron density of: **A.** Cholesterol molecules shown with a F_o-F_c electron density contoured at 2σ omitting the lipid from phase calculation, palmitic acid is also shown. **B.** Helix-kinked region with 2F_o-F_c electron density contoured at 1.5σ.